

Small-scale turbulent dynamo in astrophysical environments: nonlinear dynamo and dynamo in a partially ionized plasma

Siyao Xu · Alex Lazarian

Received: date / Accepted: date

Abstract Small-scale turbulent dynamo is responsible for the amplification of magnetic fields on scales smaller than the driving scale of turbulence in diverse astrophysical media. Most earlier dynamo theories concern the kinematic regime and small-scale magnetic field amplification. Here we review our recent progress in developing the theories for the nonlinear dynamo and the dynamo regime in a partially ionized plasma. The importance of reconnection diffusion of magnetic fields is identified for both the nonlinear dynamo and magnetic field amplification during gravitational contraction. For the dynamo in a partially ionized plasma, the coupling state between neutrals and ions and the ion-neutral collisional damping can significantly affect the dynamo behavior and the resulting magnetic field structure. We present both our analytical predictions and numerical tests with a two-fluid dynamo simulation on the dynamo features in this regime. In addition, to illustrate the astrophysical implications, we discuss several examples for the applications of the dynamo theory to studying magnetic field evolution in both preshock and postshock regions of supernova remnants, in weakly magnetized molecular clouds, during the (primordial) star formation, and during the first galaxy formation.

Keywords Magnetohydrodynamics in astrophysics · Turbulence plasma · Plasma dynamos

S.X. acknowledges the support for this work provided by NASA through the NASA Hubble Fellowship grant # HST-HF2-51473.001-A awarded by the Space Telescope Science Institute, which is operated by the Association of Universities for Research in Astronomy, Incorporated, under NASA contract NAS5-26555. A.L. acknowledges the support of the NASA TCAN 144AAG1967. The Flatiron Institute is supported by the Simons Foundation.

Siyao Xu
Institute for Advanced Study, 1 Einstein Drive, Princeton, NJ 08540, USA; Hubble Fellow,
E-mail: sxu@ias.edu

Alex Lazarian
Department of Astronomy, University of Wisconsin, 475 North Charter Street, Madison, WI 53706, USA;
lazarian@astro.wisc.edu
Center for Computation Astrophysics, Flatiron Institute, 162 5th Ave, New York, NY 10010, USA

1 Introduction

Both turbulence and magnetic fields are ubiquitous in astrophysical plasmas, and they actively participate in diverse astrophysical processes, including the star formation, cosmic ray propagation, and magnetic reconnection and particle acceleration in high-energy astrophysical environments [1, 2, 3]. Turbulence is believed to be responsible for the amplification and maintenance of cosmic magnetic fields via the “small-scale” turbulent dynamo mechanism [4]. It refers to the amplification of magnetic fields due to the presence of turbulence on scales below the driving scale of turbulence. As the evidence for the magnetic field amplification via small-scale turbulent dynamo, the measured magnetic energy spectra in diverse astrophysical media over a vast range of length scales conform to the same spectral shape as the turbulent energy (e.g., [5, 45, 46]). The dynamo amplification of magnetic fields and its implications have been studied in diverse contexts, including the large-scale structure formation [6, 7, 8, 9], (primordial) star formation and galaxy formation [10, 11, 12, 13].

In astrophysical reality, the evolution and properties of magnetic fields are determined by both the dynamo growth and diffusion of magnetic fields. Given drastically different conditions of astrophysical systems, the turbulence parameters (e.g., driving scale, injected turbulent velocity) and plasma parameters (e.g., magnetic Prandtl number, which is the ratio of viscosity to magnetic diffusivity (proportional to resistivity), ionization fraction) for describing the dynamo and diffusion processes can differ by many orders of magnitude between various systems [4]. By contrast, numerical simulations of turbulent dynamo only cover a small range of turbulence and plasma parameters due to the limited numerical resolution [14]. Therefore, it is necessary to develop theories of turbulent dynamo applicable to different physical regimes and astrophysical conditions, which can also provide the recipe of the subgrid dynamo physics for large-scale simulations [8].

Most earlier theoretical studies on turbulent dynamo focused on its kinematic regime with negligible magnetic back reaction [15, 16, 17, 18, 19]. For the kinematic regime of dynamo, the dynamo growth of magnetic fields and the magnetic field structure are sensitive to the plasma parameters, including both the ionization fraction [17, 20] and the magnetic Prandtl number [21, 22]. For astrophysical settings involving large length scales and long timescales, the kinematic dynamo alone is insufficient to explain the dynamo evolution of magnetic fields and their dynamical roles in the multi-scale astrophysical processes. With the growth of magnetic energy, the magnetic back reaction on turbulence becomes significant and the dynamo enters the nonlinear regime. Numerical simulations reveal that the dynamo in the nonlinear regime has distinctive characteristics [23, 24, 6, 25, 26]. Instead of an exponential growth of magnetic energy, the magnetic energy grows linearly with time with an inefficient dynamo growth rate. The resulting magnetic energy spectrum peaks at a large length scale instead of the resistive scale as for the kinematic dynamo [24, 4].

Xu & Lazarian (2016) [27] (hereafter XL16) developed an analytical theory of nonlinear turbulent dynamo and found the importance of reconnection diffusion (RD) of magnetic fields in a proper formulation of the nonlinear dynamo. RD of magnetic fields occurs for magnetic fields in the presence of turbulence. When magnetic fields are mixed by turbulence, the turbulent motion brings magnetic fields with different

directions into contact and magnetic reconnection happens. This turbulence induced magnetic reconnection, i.e., turbulent reconnection, is an intrinsic part of magnetohydrodynamic (MHD) turbulence [28, 3]. It enables the RD of turbulent magnetic fields, which otherwise can only have wave-like oscillations [29, 30, 31]. We note that RD is different from the turbulent diffusion that is commonly used in mean-field dynamos. While the turbulent diffusion usually describes the diffusion of the weak magnetic field that can be treated as a passive vector, the RD describes the diffusion of the magnetic field that has a significant back reaction on turbulence. In the nonlinear stage of dynamo, RD dominates over other microphysical diffusion effects arising from plasma processes, e.g., ambipolar diffusion, resistive diffusion, and it accounts for both the inefficient growth of magnetic energy and the large correlation scale of amplified magnetic fields that cannot be explained by the kinematic dynamo.

Besides the nonlinear regime, XL16 also studied the kinematic dynamo at a large and small magnetic Prandtl number, and at different ionization fractions. They found new regimes of kinematic dynamo, including the transitional stage in a high-Prandtl number medium with the shift of the correlation length of magnetic fields from the resistive scale to the viscous scale, and the damping stage of dynamo in a weakly ionized medium (see also [22]). XL16 predictions on the dynamo behavior resulting from the weak coupling between neutrals and ions at a low ionization fraction have been numerical confirmed by the two-fluid dynamo simulation [32].

Turbulent dynamo naturally occurs when the turbulent energy exceeds the magnetic energy in astrophysical media, provided that there is a non-zero seed magnetic field. The seed field can be of primordial origin ([33, 34, 35, 36, 37]). The XL16 theory has a broad range of astrophysical applications for studying the evolution and structure of magnetic fields, e.g., in supernova remnants and the implications on cosmic ray diffusion and acceleration [38], in gravitational collapse and primordial star formation [12, 13], and in weakly ionized interstellar phases [39, 32]. In this review, we focus on the nonlinear turbulent dynamo (Section 2) and the dynamo in a partially ionized medium (Section 3) formulated in XL16. We also provide examples of their applications to studying magnetic field amplification in a variety of astrophysical processes and astrophysical environments collected from our recent studies.

2 Nonlinear turbulent dynamo

Turbulent stretching of magnetic fields leads to the dynamo amplification of magnetic fields. We note that shock compression and gravitational compression in a contracting flow, as well as turbulent compression in compressible MHD turbulence, can also lead to amplification of magnetic fields. Here we distinguish the stretching of magnetic fields by turbulent shear from other mechanisms for magnetic field amplification, and only consider the former process as small-scale turbulent dynamo.

In the kinematic regime of turbulent dynamo with a negligible back reaction of magnetic fields, the dynamo theory was developed by [16] (see also [40, 17, 41]). When the magnetic back reaction becomes significant, we need to deal with the nonlinear turbulent dynamo. Nonlinear turbulent dynamo is characterized by the energy

equipartition between turbulence and magnetic fields within the inertial range of turbulence.

2.1 Theoretical formulation of nonlinear turbulent dynamo

Magnetic reconnection in the presence of turbulence has the reconnection rate dependent on turbulence properties. This is known as the turbulent reconnection of magnetic fields [28]. Turbulent reconnection is an intrinsic part of MHD turbulent cascade and enables the turbulent motions of magnetic fields, which otherwise would only have wave-like oscillations. The turbulent reconnection theory has been tested both numerically and observationally, with a broad range of applications in a variety of astrophysical environments (see the recent review by [3]).

Diffusion of magnetic fields relative to plasma as a result of turbulent reconnection is termed as “reconnection diffusion (RD)” [29,30,31]. It has been applied in the context of star formation and well explains observations (e.g.,[42,43,44]). Despite its importance, RD was disregarded in earlier studies of nonlinear turbulent dynamo. We stress that although some microphysical effects, e.g., ambipolar diffusion, were discussed in the literature as nonlinear effects [17,18], the “nonlinear” dynamo considered here is characterized by the energy equipartition between turbulence and magnetic fields and by the development of MHD turbulence because of the dynamical effect of magnetic fields on turbulence.

The dynamo growth rate is determined by both the turbulent stretching of magnetic fields and diffusion of magnetic fields, as the former amplifies magnetic fields, and the latter causes loss of magnetic fields. As another important characteristic of nonlinear dynamo, RD of magnetic fields dominates over other diffusion effects arising from plasma microphysics, e.g., ambipolar diffusion (related to ionization fraction), resistive diffusion (related to magnetic Prandtl number). Otherwise the MHD turbulence would be suppressed by microscopic diffusion effects on all length scales, and the dynamo would not be in the nonlinear regime. Therefore, the dynamo growth rate of nonlinear dynamo is only dependent on the parameters of turbulence.

XL16 derived the nonlinear dynamo theory and found that the magnetic energy \mathcal{E} grows linearly with time,

$$\mathcal{E} = \mathcal{E}_{\text{cr}} + \frac{3}{38}\epsilon(t - t_{\text{cr}}), \quad (1)$$

where \mathcal{E}_{cr} is the magnetic energy at the beginning of the nonlinear stage at the time $t = t_{\text{cr}}$. In a system with the initial magnetic energy \mathcal{E}_{cr} in equipartition with the turbulent energy at some length scale within the inertial range of turbulence, that is, the turbulence is super-Alfvénic (see Section 2.2), we have $t_{\text{cr}} = 0$. In a system with an initially very weak magnetic field, the turbulent dynamo is first in the kinematic regime until the energy equipartition between turbulence and magnetic field can be reached at some length scale within the inertial range. In this case, t_{cr} is given by the duration of the kinematic stage and depends on the plasma conditions (XL16). The linear dependence of \mathcal{E} on time comes from the constant energy transfer rate $\epsilon = v_k^3 k$ of turbulence. Here v_k is the turbulent velocity corresponding to the wavenumber k . The turbulent energy cascade with the turbulent kinetic energy transferred from one

eddy to the next smaller eddy has a constant energy transfer rate. Meanwhile, a small fraction $3/38$ of the turbulent energy is converted to magnetic energy within the eddy turnover time, resulting in a constant magnetic energy growth rate. The low efficiency of nonlinear dynamo growth is the consequence of reconnection diffusion. The growing magnetic energy is passed down toward smaller scales along the turbulent energy cascade. The above small growth rate of nonlinear dynamo is quantitatively consistent with that measured in nonlinear dynamo simulations by, e.g., [6, 25].

The correlation length $1/k_p$ of the stretched magnetic fields is given by the size of turbulent eddies that dominate the stretching. As the energy equipartition between turbulence and magnetic fields is reached scale by scale, the correlation length of magnetic fields increases with time (XL16),

$$k_p = \left[k_{\text{cr}}^{-\frac{2}{3}} + \frac{3}{19} \epsilon^{\frac{1}{3}} (t - t_{\text{cr}}) \right]^{-\frac{3}{2}}, \quad (2)$$

where k_{cr} is the correlation wavenumber of magnetic fields at $t = t_{\text{cr}}$. As an illustration, Fig. 1 shows the magnetic energy spectrum $M(k)$ in the nonlinear stage of dynamo with magnetic Prandtl number $P_m = 1$ and $P_m \gg 1$. $1/k_p$ is the peak scale of $M(k)$. At $k > k_p$, magnetic energy is in equipartition with turbulent energy, and $M(k)$ follows the same Kolmogorov energy spectrum as that of hydrodynamic turbulence due to reconnection diffusion. At $k < k_p$, magnetic fields are relatively weak, and $M(k)$ has the form of Kazantsev spectrum as in the kinematic regime of dynamo. The analytical expectation in XL16 agrees well with the simulations by [4]. As we discussed, the nonlinear dynamo is independent of plasma effects and thus independent of P_m . The short inertial range of turbulence seen in the dynamo simulation at $P_m = 50$ is due to the limited numerical resolution.

At the final saturation of nonlinear dynamo, magnetic energy is in approximate equipartition with the turbulent energy at the injection scale L ,

$$\mathcal{E}_{\text{sat, nl}} = \frac{1}{2} V_L^2, \quad (3)$$

where V_L is the turbulent velocity at L . The time required for the nonlinear dynamo to reach final saturation is approximately

$$\tau_{\text{nl}} \approx \frac{19}{3} \frac{L}{V_L}. \quad (4)$$

In the above expression, we assume that the turnover time of the smallest eddies are negligible compared with that of the largest eddy at L . The timescale of nonlinear dynamo is much longer than the turbulent eddy turnover time at L because of its inefficient dynamo growth. The relatively long timescale of the nonlinear dynamo and its low efficiency indicate that only a small fraction of turbulent energy contributes to the growth of magnetic energy. This result is also consistent with that in dynamo simulations in a cosmological context [6, 7, 9] and in supernova remnants (see Section 2.3).

As the observational evidence for nonlinear dynamo in astrophysical media, the large correlation length of magnetic fields and Kolmogorov spectrum of magnetic energy are indicated by magnetic field measurements in the interstellar medium (ISM) (e.g., [45]) and the intracluster medium (ICM) (e.g., [46]).

2.2 Magnetic field amplification in weakly magnetized molecular clouds

Turbulent dynamo takes place when the turbulent energy is larger than the magnetic energy. In a super-Alfvénic turbulent molecular cloud (MC) with the initial Alfvénic Mach number $M_A = V_L/V_A$ larger than unity, where $V_A = B/\sqrt{4\pi\rho}$ is the Alfvén speed, B is the magnetic field strength, and ρ is density, nonlinear dynamo occurs within the inertial range of turbulence. Turbulence in MCs can originate from the global cascade of turbulence driven by supernova explosions [47].

As an illustration, Fig. 2 shows the evolution of magnetic energy spectrum due to nonlinear turbulent dynamo in an initially weakly magnetized MC. It follows the same Kolmogorov form as the turbulent spectrum. l_A corresponds to the energy equipartition scale and the peak scale of the evolving magnetic energy spectrum. It increases with time (Eq. (2)) until reaching $l_A = L$ at the final saturation, and the turbulence becomes trans-Alfvénic with $M_A = 1$. $k_{\text{dam},\perp}$ is the perpendicular ion-neutral collisional damping wavenumber in a weakly ionized medium (see Section 3), and k_ν is the viscous wavenumber due to neutral viscosity. The ion-neutral collisional damping usually dominates over the neutral viscous damping in a weakly ionized medium [48, 49, 39].

We note that if the cloud lifetime is comparable to the turbulent crossing time [50], then as the inefficient nonlinear dynamo has the timescale much longer than the largest eddy turnover time (Eq. (4)), final energy equipartition between turbulence and magnetic fields at L may not be reached in an initially highly super-Alfvénic MC. It means that the turbulence in the MC would stay super-Alfvénic during the star formation process. This finding can have important implications for studying the role of magnetic fields in star formation [51].

2.3 Magnetic field amplification in supernova remnants: postshock region

Strong magnetic fields in supernova remnants (SNRs) are inferred from observations (e.g., [52, 53, 54]) and are also required for confining cosmic ray particles for acceleration. The above nonlinear dynamo theory has been applied to studying magnetic field amplification in the SNR postshock region in [38]. Different from the interstellar turbulence, the turbulence in the SNR postshock region is driven by the interaction between supernova shocks and interstellar density inhomogeneities. The driving scale is comparable to the size of density clumps in the upstream ISM.

In [38], the magnetic field amplification based on the nonlinear dynamo theory is compared with that measured in shock simulations [55] (see Fig. 3). The linear-in-time growth of magnetic energy with a small dynamo growth rate as expected for nonlinear dynamo theory is seen from the simulated temporal evolution of magnetic fields (Fig. 3(a)). The maximum field strength is determined by the injected turbulent velocity, which depends on the shock velocity in different numerical models. The position where the nonlinear dynamo saturates and the magnetic field reaches its highest strength (indicated by the vertical dashed line in Fig. 3(b)) is determined by the shock velocity and the nonlinear dynamo timescale. The long timescale of the

inefficient nonlinear dynamo well explains the position of the maximum magnetic field, which is far away from the shock front.

Both results naturally explain the X-ray hot spots detected at more than 0.1 pc in the SNR postshock region, which suggest the presence of magnetic field of ~ 1 mG far behind the shock front [56,57].

2.4 Magnetic field amplification during gravitational collapse

In a weakly magnetized and gravitationally collapsing system, magnetic fields are amplified not only by turbulent dynamo, but also by gravitational compression. The growth of magnetic energy in this scenario can be described as [13]

$$\mathcal{E} = \frac{3}{38}\epsilon_0 C^{\frac{4\alpha}{19}} \int_{t_{\text{cr}}}^t C^{-\frac{3}{2} - \frac{4\alpha}{19}} dt + \mathcal{E}_{\text{cr}} C^{\frac{4\alpha}{19}}, \quad (5)$$

where $C = r/r_0$ is defined as the compression factor, r_0 is the initial radius of the collapsing sphere, and r is the radius at time t . ϵ_0 is the initial energy transfer rate of turbulence, and $\alpha = -1$ for isotropic compression. The above formula can recover the expression in Eq. (1) at $C = 1$ for nonlinear dynamo without gravitational compression. The correlation wavenumber of the amplified magnetic fields evolves as [13]

$$k_p = \left[\frac{3}{19}\epsilon_0^{\frac{1}{3}} C^{1+\frac{4\alpha}{19}} \int_{t_{\text{cr}}}^t C^{-\frac{3}{2} - \frac{4\alpha}{19}} dt + 2\epsilon_0^{-\frac{2}{3}} \mathcal{E}_{\text{cr}} C^{1+\frac{4\alpha}{19}} \right]^{-\frac{3}{2}}. \quad (6)$$

The correlation length $1/k_p$ becomes comparable to the driving scale of turbulence at the full saturation of nonlinear dynamo.

For the free-fall collapse of a uniform sphere [58], we consider the compression factor as [59,12],

$$C \approx \left(1 - \left(\frac{t}{t_{ff}} \right)^2 \right)^{\frac{2}{3}}, \quad (7)$$

where t_{ff} is the initial free-fall time of the sphere. In this case, \mathcal{E} , normalized by the turbulent energy $V_L^2/2$ at L , evolves as [13]

$$\begin{aligned} \frac{\mathcal{E}}{\frac{1}{2}V_L^2} &\approx \frac{3}{19}\sqrt{\frac{3}{32}} C^{\frac{4\alpha}{19}} \int_{\frac{t_{\text{cr}}}{t_{ff}}}^{\frac{t}{t_{ff}}} \left(1 - \left(\frac{t}{t_{ff}} \right)^2 \right)^{\beta} d\left(\frac{t}{t_{ff}} \right) \\ &\quad + \frac{\mathcal{E}_{\text{cr}}}{\frac{1}{2}V_L^2} C^{\frac{4\alpha}{19}} \end{aligned} \quad (8)$$

$$\approx \frac{3}{19}\sqrt{\frac{3}{32}} C^{\frac{4\alpha}{19}} \sqrt{1 - C^{\frac{3}{2}}} + \frac{\mathcal{E}_{\text{cr}}}{\frac{1}{2}V_L^2} C^{\frac{4\alpha}{19}}, \quad (9)$$

where Eq. (9) is its approximate form at a short time. Fig. 4 shows the evolution of the normzlied \mathcal{E} as a function of t and density ρ , where ρ_0 is the initial density. The growth of \mathcal{E} is initially dominated by the nonlinear turbulent dynamo when the

change of ρ is insignificant. With the rapid growth of ρ at a later time, the gravitational compression becomes the dominant effect on amplifying magnetic fields. The scaling becomes slightly steeper than

$$\mathcal{E} \propto C^{\frac{4\alpha}{19}} \propto \rho^{-\frac{4\alpha}{57}}. \quad (10)$$

The relation of C to ρ is given by

$$\frac{\rho}{\rho_0} = \frac{r_0^3}{r^3} = C^{-3}. \quad (11)$$

We note that the slope $4\alpha/19$ is derived based on the Kolmogorov spectrum of turbulent energy and the Kazantsev spectrum of magnetic energy (see also e.g., [40,41] for a different form of Kazantsev spectrum), and is independent of the detailed model for collapse.

As a comparison with the flux-freezing scaling, we also present the result in Fig. 4 for compression alone under the freezing-in condition,

$$\frac{\mathcal{E}}{\frac{1}{2}V_L^2} = \frac{\mathcal{E}_{\text{cr}}}{\frac{1}{2}V_L^2} C^\alpha. \quad (12)$$

It grows steeply with ρ . By contrast, when the reconnection diffusion of magnetic field is taken into account, \mathcal{E} has a much weaker dependence on ρ . The removal of magnetic flux during compression has been numerically demonstrated by, e.g., [42]. Despite the additional magnetic field amplification via gravitational compression, the balance between the growth of magnetic fields and the reconnection diffusion of magnetic fields still stands, and the growth ceases when \mathcal{E} reaches equipartition with the turbulent energy of the largest eddy at L .

Fig. 5 shows the evolution of correlation length $l_p = 1/k_p$ as a function of ρ . As l_p is also the energy equipartition scale, it is related to \mathcal{E} by

$$\mathcal{E} = \frac{1}{2}v_p^2 = \frac{1}{2}L^{-\frac{2}{3}}V_L^2k_p^{-\frac{2}{3}}, \quad (13)$$

where v_p is the turbulent velocity at k_p ,

$$v_p = V_L(k_pL)^{-\frac{1}{3}}. \quad (14)$$

Eq. (13) can be rewritten as

$$\frac{l_p}{L} = \left(\frac{\mathcal{E}}{\frac{1}{2}V_L^2} \right)^{\frac{3}{2}}. \quad (15)$$

With the growth of \mathcal{E} , l_p/L first increases rapidly with ρ and then increases gradually with the scaling close to (Eq. (10))

$$\frac{l_p}{L} \propto \mathcal{E}^{\frac{3}{2}} \propto \rho^{-\frac{2\alpha}{19}} \quad (16)$$

up to unity.

By comparing with the evolution of magnetic field strength $B \propto \sqrt{\mathcal{E}\rho}$ as a function of density numerically measured by [10] from simulations on magnetic field

amplification during gravitational collapse, the analytical expectation for nonlinear dynamo in a collapsing system (dashed line in Fig. 6) agrees well with the numerical result. It demonstrates the importance of reconnection diffusion and the breakdown of flux-freezing assumption. Table 1 clearly shows the differences between the cases with reconnection diffusion and flux-freezing for the evolution of magnetic fields during the gravitational collapse. This result is important for studying the dynamics of magnetic fields and their effects on the primordial star formation [12, 60].

Table 1 Comparison between the cases with reconnection diffusion and flux-freezing. From [13].

	Reconnection diffusion	Flux-freezing
Magnetic energy spectrum	Kazantsev spectrum ($k < k_p$) Kolmogorov spectrum ($k_p < k < k_d$)	Kazantsev spectrum ($k < k_d$)
Magnetic field structure	Turbulent structure	Folded structure
Correlation length of magnetic fields	$1/k_p$ (equipartition scale)	$1/k_d$ (dissipation scale)
Dependence of B on ρ under compression	$B \propto \rho^{\frac{2}{5\tau} + \frac{1}{2}}$ (nonlinear) $B \propto \rho^{\frac{1}{2}}$ (saturated)	$B \propto \rho^{2/3}$

We caution that for comparison with dynamo simulations in a collapsing system, given the limited numerical resolution, it is very challenging to numerically resolve the entire turbulent cascade down to the smallest turbulent eddies. As the fastest dynamo rate is determined by the turnover rate of the smallest eddies, the dynamo growth is affected and the kinematic dynamo in simulations is prolonged [12] (also see Fig. 6). In addition, here we adopt a Kolmogorov turbulent cascade by assuming the turbulent cascade is faster than the gravitational contraction. In the central collapsing region, when the local contraction becomes faster than the turbulent cascade, additional turbulence can be driven with the gravitational energy converted to turbulent energy, which can have a different scaling from the Kolmogorov one [61, 62, 63].

3 Turbulent dynamo in a partially ionized plasma

Partially ionized plasmas are very common in astrophysical environments, such as molecular clouds and protoplanetary disks. In a partially ionized medium, the coupling between magnetic fields and neutrals is determined by the coupling between neutrals and ions via their collisions. Table 2 lists different coupling regimes for both MHD turbulence with strong magnetic fields and turbulent dynamo with initially weak magnetic fields. Here ν_{in} and ν_{ni} are ion-neutral and neutral-ion collisional frequencies. In a weakly ionized medium, there is $\nu_{in} > \nu_{ni}$. ω_A is the Alfvén wave frequency, and Γ_l is the dynamo stretching rate at length scale l . When the neutral-ion collisions are infrequent, the relative drift between the two species causes diffusion of

magnetic fields, i.e., ambipolar diffusion, and inefficient dynamo growth of magnetic fields. In a weakly ionized medium, the ion-neutral collisional damping is also the dominant damping effect for magnetic fluctuations [48, 49, 39].

Table 2 Coupling regimes in MHD turbulence and turbulent dynamo. From [32].

Coupling regime	Strong coupling	Weak coupling	Decoupling
MHD turbulence	$\omega_A < \nu_{ni}$	$\nu_{ni} < \omega_A < \nu_{in}$	$\omega_A > \nu_{in}$
Turbulent dynamo	$\Gamma_l < \nu_{ni}$	$\nu_{ni} < \Gamma_l < \nu_{in}$	$\Gamma_l > \nu_{in}$

3.1 Turbulent dynamo in a weakly ionized medium

XL16 introduced a parameter

$$\mathcal{R} = \frac{6}{\xi_n} \frac{\nu_{ni}}{\Gamma_\nu}, \quad (17)$$

where ξ_n is the neutral fraction, ν_{ni} is the neutral-ion collisional frequency, and Γ_ν is the dynamo stretching rate at the viscous scale. \mathcal{R} depends on the ionization fraction and reflects the strength of neutral-ion coupling. At $\mathcal{R} > 1$ with a high ionization fraction, the neutral-ion coupling is sufficiently strong for the turbulent motions carried by neutrals at the viscous scale to efficiently stretch and amplify magnetic fields. At $\mathcal{R} < 1$ with a low ionization fraction, the neutral-ion coupling is weak, which results in ineffective turbulent stretching and inefficient dynamo growth of magnetic fields.

XL16 found that the turbulent dynamo at $\mathcal{R} < 1$ is characterized by a unique damping stage of dynamo. During the damping stage, magnetic energy grows as

$$\sqrt{\mathcal{E}_M} = \sqrt{\mathcal{E}_{M1}} + \frac{3}{23} \mathcal{C}^{-\frac{1}{2}} L^{-\frac{1}{2}} V_L^{\frac{3}{2}} (t - t_1), \quad (18)$$

where \mathcal{E}_{M1} is the magnetic energy at the beginning of the damping stage at $t = t_1$, and $\mathcal{C} = \xi_n / (3\nu_{ni})$ is related to the ionization fraction. It means that the magnetic field strength $B \propto \sqrt{\mathcal{E}_M}$ grows linearly with time, and the growth rate depends on the ionization fraction. We note that due to the weak coupling between neutrals and ions, the growth of \mathcal{E}_M mainly comes from the turbulent energy contained in ions.

As shown in Fig. 7, the magnetic energy spectrum during the damping stage is cut off at the ion-neutral collisional damping scale $l_d = 1/k_d$, where significant damping of magnetic fluctuations takes place. With the growth of magnetic energy, l_d evolves as

$$l_d = \left(l_{d1}^{\frac{2}{3}} + \frac{3}{23} L^{-\frac{1}{3}} V_L (t - t_1) \right)^{\frac{3}{2}}, \quad (19)$$

where l_{d1} is the damping scale at $t = t_1$. As l_d is also the correlation length of the amplified magnetic fields. It means that the magnetic fields have an increasing correlation length during the damping stage.

Table 3 Simulation parameters

R	L	ρ_i/ρ_n	V_{rms}	c_s	M_{Ai0}
1024^3	512	1.26×10^{-3}	0.2	1	17.7

3.2 Numerical test with two-fluid dynamo simulation

To numerically test the turbulent dynamo theory in a weakly ionized medium, it is necessary to carry out a two-fluid simulation that treats the dynamics of neutrals and ions separately. [32] performed a 3D high-resolution two-fluid dynamo simulation to solve the following equations [64] by using the two-fluid RIEMANN code [65,66],

$$\begin{aligned}
\frac{\partial \rho_i}{\partial t} + \nabla \cdot (\rho_i \mathbf{v}_i) &= 0, \\
\frac{\partial \mathbf{v}_i}{\partial t} + (\mathbf{v}_i \cdot \nabla) \mathbf{v}_i &= -c_s^2 \nabla \ln \rho_i - \frac{1}{4\pi} \mathbf{B} \times (\nabla \times \mathbf{B}) \\
&\quad - \gamma_d \rho_n (\mathbf{v}_i - \mathbf{v}_n), \\
\frac{\partial \mathbf{B}}{\partial t} &= \nabla \times (\mathbf{v}_i \times \mathbf{B}), \\
\frac{\partial \rho_n}{\partial t} + \nabla \cdot (\rho_n \mathbf{v}_n) &= 0, \\
\frac{\partial \mathbf{v}_n}{\partial t} + (\mathbf{v}_n \cdot \nabla) \mathbf{v}_n &= -c_s^2 \nabla \ln \rho_n - \gamma_d \rho_i (\mathbf{v}_n - \mathbf{v}_i),
\end{aligned} \tag{20}$$

where \mathbf{v}_i and \mathbf{v}_n are the velocities of the ionized and neutral fluids, \mathbf{B} is the magnetic field, c_s is the sound speed, ρ_i and ρ_n are ion and neutral mass densities, and γ_d is the drag coefficient [67]. Table 3 lists the parameters used in the simulation, where R is the numerical resolution, and V_{rms} is the injected turbulent velocity at the driving scale L . The initial large Alfvén Mach number M_{Ai0} corresponds to the initial weak magnetic field for a dynamo simulation. The ionization fraction should be sufficiently small to ensure that neutrals are weakly coupled with ions and the dynamo is in the damping regime.

Fig. 8 shows the numerically measured magnetic energy spectrum at different times of the simulation. The initial uniform magnetic field is aligned along the x -direction. The smallest turbulent eddies have the fastest dynamo stretching rate. So the peak scale of the initial magnetic energy spectrum $M(k, t)$ first shifts to smaller scales. Then with the growth of magnetic energy, the ion-neutral collisional damping effect becomes more significant. Accordingly, the damping scale l_d , where $M(k, t)$ peaks, increases with time (see Eq. (19)). At $t = 7.49 \tau_{\text{eddy}}$, where τ_{eddy} is the eddy-turnover time at L , the amplified magnetic fields have a large correlation length. The smaller-scale magnetic fluctuations on scales less than l_d are suppressed due to ion-neutral collisional damping. This can be clearly seen from the magnetic field structure shown in Fig. 9.

As an important characteristic of the turbulent dynamo in a weakly ionized medium, the analytically predicted linear-in-time growth of magnetic field strength B during

the damping stage of dynamo (see Eq. (18)) is also numerically confirmed in [32]. As displayed in Fig. 10, after the exponential growth of B during the first τ_{eddy} , B grows linearly with time in the subsequent damping stage. The effective Alfvén speed $V_{A,\text{eff}}$ defined in [32] is proportional to B .

The above numerically tested dynamo theory in a weakly ionized medium can be generally applied to studying magnetic field amplification in weakly ionized astrophysical media. The dynamo growth of magnetic fields and their properties depend on the turbulence parameters and ionization fraction in the local environment.

3.3 Magnetic field amplification in supernova remnants: preshock region

Supernova shocks are believed to be the accelerators of Galactic CRs [68], and magnetic fields much stronger than the interstellar magnetic fields are required for the particle confinement and acceleration (see Section 2.3). Magnetic field amplification in the preshock region in the literature is usually attributed to the CR-driven instabilities [69]. More recently, turbulent dynamo has also been invoked as a different mechanism for magnetic field amplification in the preshock region [70, 71, 72]. The upstream turbulence can be induced by the interaction between the CR pressure gradient in the shock precursor and the upstream density inhomogeneities [70, 71]. Density inhomogeneities are very common in the interstellar medium as suggested by observations [73, 74]. [38] took into account the effect of ion-neutral collisional damping in a partially ionized medium and reexamined the turbulent dynamo in the shock precursor.

For supernova shocks propagating in the multi-phase interstellar medium, including the warm neutral medium (WNM), cold neutral medium (CNM), MCs, and dense cores (DC) (Table 4), by considering the driving condition of the precursor turbulence as

$$L = 0.1 \text{ pc}, \quad V_L = 10^3 \text{ km s}^{-1}, \quad (21)$$

where L is the characteristic scale of the density structure in cold interstellar phases [75, 76] and V_L is of the order of shock velocity, [32] found that the turbulent dynamo in the shock precursor is entirely in the damping stage as shown in Fig. 11. Here n_H and n_e are number densities of the atomic hydrogen and electrons, and T is the temperature [77]. The timescale of the dynamo τ_{dam} ,

$$\tau_{\text{dam}} = \frac{23}{3} \left(\frac{L}{V_L} - \Gamma_\nu^{-1} \right), \quad (22)$$

where Γ_ν is the dynamo stretching rate at the viscous scale, and the strength B_{dam} and correlation length $l_{d,\text{cr}}$ of magnetic fields reached at the end of dynamo are all listed in Table 4. Magnetic fields of the order of $100 \mu\text{G}$ near the shock front are indicated by observations (e.g., [78, 79, 53, 54]).

As τ_{dam} is small compared with the precursor crossing time $(c/v_{\text{sh}})L/V_L$, where c and v_{sh} are the light speed and shock propagation speed, the dynamo-amplified magnetic fields with the correlation length L can be present in the shock precursor.

The diffusion of CRs is significantly affected by the structure of magnetic fields. For CRs streaming along the dynamo-amplified magnetic fields in a weakly ionized

medium, their effective mean free path is determined by the ion-neutral collisional damping scale. The maximum energy of CRs that can be confined in the case of the shock propagation in an MC is

$$E_{\text{CR,max}} = eB_{\text{dam}}L \approx 38 \text{ PeV}. \quad (23)$$

Different from the magnetic field amplification induced by CR-driven instabilities, the magnetic fields amplified by turbulent dynamo have the correlation length independent of CR gyroradius. Both mechanisms should be taken into account when studying CR diffusion and acceleration at supernova shocks.

For supernova shocks propagating through the partially ionized interstellar medium, we discuss the turbulent dynamo as a mechanism for amplifying the preshock magnetic fields. Given the parameters adopted here, Eq. (23) provides an estimate for the maximum energy of CRs that the dynamo-amplified magnetic fields can confine. The detailed modeling of shock acceleration of CRs that involves the dynamo-amplified magnetic fields and the dependence of the maximum CR energy on the local interstellar environment require further studies. We also note that the recent observations of SNRs suggest that the maximum energy of accelerated CRs is below 1 PeV (e.g., [80,81]). In these observed SNRs, the magnetic field amplification may not be very efficient.

Table 4 Turbulent dynamo in the shock precursor in the multi-phase interstellar medium. From [32].

	WNM	CNM	MC	DC
$n_{\text{H}}[\text{cm}^{-3}]$	0.4	30	300	10^4
n_e/n_{H}	0.1	10^{-3}	10^{-4}	10^{-6}
$T[\text{K}]$	6000	100	20	10
$l_{d,\text{cr}} [\text{pc}]$			0.1	
$\tau_{\text{dam}}[\text{kyr}]$			0.75	
$B_{\text{dam}} [\mu \text{ G}]$	79.1	56.6	415.2	138.2

3.4 Multiple evolutionary stages of turbulent dynamo in a partially ionized medium

Besides the damping stage of dynamo, depending on the ionization fraction and initial magnetic field strength, the turbulent dynamo in a partially ionized medium can have multiple evolutionary stages with distinctive growth behavior of magnetic fields. Tables 5-7 present the dependence of magnetic energy \mathcal{E} on time t in different evolutionary stages of turbulent dynamo in a partially ionized medium corresponding to different ranges of \mathcal{R} (Eq. (17)). \mathcal{E}_0 is the initial magnetic energy, and $E_{k,\nu}$ is the turbulent energy at the viscous scale. The detailed derivation and analysis of each evolutionary stage can be found in XL16.

Table 5 $\mathcal{R} < 1$. From [39].

Stages	Dissipation-free	Viscous	Damping	Nonlinear
\mathcal{E}	$\sim e^{2\Gamma_\nu t}$	$\sim e^{\frac{1}{3}\Gamma_\nu t}$	$\sim t^2$	$\sim t$

Table 6 $1 < \mathcal{R} < 5^{\frac{4}{5}} \left(\frac{E_{k,\nu}}{\varepsilon_0} \right)^{\frac{1}{2}}$. From [39].

Stages	Dissipation-free	Viscous	Transitional	Nonlinear
\mathcal{E}	$\sim e^{2\Gamma_\nu t}$	$\sim e^{\frac{1}{3}\Gamma_\nu t}$	$E_{k,\nu}$	$\sim t$

Table 7 $\mathcal{R} \geq 5^{\frac{4}{5}} \left(\frac{E_{k,\nu}}{\varepsilon_0} \right)^{\frac{1}{2}}$. From [39].

Stages	Dissipation-free	Transitional	Nonlinear
\mathcal{E}	$\sim e^{2\Gamma_\nu t}$	$E_{k,\nu}$	$\sim t$

As an illustration, XL16 considered the magnetic field amplification in the first galaxies. The parameters for the turbulence driving and physical conditions are taken from [82, 11]. The dynamo amplification of magnetic field strength B and the evolution of the correlation length l_p of magnetic fields are displayed in Fig. 12. Their values in corresponding evolutionary stages are provided in Table 8. t_{ff} is the free-fall time of the system. The growth of B is inefficient in both damping stage and nonlinear stage, but l_p increases from the viscous scale up to the driving scale of turbulence during these two stages. The dashed lines in Fig. 12(a) and Fig. 12(b) indicate the magnetic field strength when the magnetic energy is in equipartition with the turbulent energy at the viscous scale and the viscous scale, respectively.

As the new turbulent dynamo theory was adopted, different from earlier studies by, e.g., [82, 11], XL16 identified multiple evolutionary stages including the new damping stage of dynamo. For the nonlinear dynamo, its inefficiency due to reconnection diffusion of magnetic fields leads to a much more prolonged evolutionary stage compared with earlier studies (see Section 2). We note that the timescale of nonlinear stage of dynamo can be even longer than t_{ff} . This result can have important implications for the effect of magnetic fields during the formation and evolution of the first galaxies.

4 Summary

As two sides of the same coin, turbulent reconnection and turbulent dynamo are two fundamental components of MHD turbulence. They result in the energy exchange between turbulence and magnetic fields. For the critical balanced MHD turbulence [83] generated in nonlinear turbulent dynamo, there is a balance between the dynamo growth and RD of magnetic fields at all length scales of the MHD turbulence.

Table 8 $t_{\text{ff}} = 16.3$ Myr, $\mathcal{R} = 0.006$. From XL16.

$B(t)$	t [Myr]	l_p [pc]	B [G]
Dissipation-free ($\sim e^{\Gamma\nu t}$)	1.1×10^{-2}	6.0×10^{-9}	1.2×10^{-12}
Viscous ($\sim e^{\frac{1}{6}\Gamma\nu t}$)	4.4×10^{-2}	1.2×10^{-4}	2.5×10^{-8}
Damping ($\sim t$)	7.3×10^{-1}	2.5×10^{-1}	3.9×10^{-6}
Nonlinear ($\sim \sqrt{t}$)	31.1	1.0×10^2	2.9×10^{-5}

Therefore, RD of magnetic fields is indispensable for studying the nonlinear turbulent dynamo. It dominates over all other diffusion effects arising from plasma processes and accounts for the inefficiency of nonlinear dynamo, as well as the large correlation length of amplified magnetic fields.

By extending the nonlinear dynamo theory to include the gravitational compression, we see that both turbulence and compression contribute to the growth of magnetic fields, and the latter becomes the dominant process with the increase of density. There is a weak dependence of magnetic energy on density during contraction. This significant deviation from the flux-freezing scaling between magnetic energy and density is attributed to the RD in ideal MHD turbulence. The breakdown of the flux freezing is important for understanding the magnetic flux problem and its implications for the (primordial) star formation.

In a partially ionized plasma, the ionization fraction and the two-fluid (neutrals and ions) effect should be taken into account when studying turbulent dynamo. When neutrals and ions are weakly coupled in a weakly ionized plasma, turbulent dynamo has a unique damping stage with significant ion-neutral collisional damping and a large cutoff scale of magnetic energy spectrum. Due to the weak neutral-ion coupling, the growing magnetic energy mainly comes from the turbulent energy carried by ions, which is a small fraction of the total turbulent energy contained in two fluids. XL16 analytical predictions on the damping stage of dynamo are numerically tested with a two-fluid dynamo simulation, which demonstrates the linear-in-time growth of magnetic field strength and the increasing ion-neutral collisional damping scale as the correlation length of magnetic fields.

Depending on the ranges of plasma parameters including magnetic Prandtl number and ionization fraction, the driving condition of turbulence, and the initial magnetic energy, turbulent dynamo can have different physical regimes and multiple evolutionary stages, and thus the XL16 dynamo theory can be applied to a variety of astrophysical systems. For instance, the nonlinear dynamo can account for the magnetic field evolution and distribution in the postshock region of a SNR, which explains the strong magnetic fields seen in shock simulations and indicated by X-ray observations. The damping stage of dynamo in the partially ionized preshock region serves as an alternative mechanism for magnetic field amplification apart from the CR-driven instabilities. The dynamo-amplified magnetic fields, which are also damped by ion-neutral collisional damping, can significantly affect the diffusion and thus the confinement of CRs at the shock. As the preshock dynamo depends on the upstream interstellar environment, the strength and correlation length of the amplified magnetic fields, and

the maximum energy of CRs that can be confined by the magnetic fields can also have dependence on the local interstellar environment, which varies significantly in different interstellar phases.

Given the limited numerical resolution, it is very challenging to realistically simulate the astrophysical dynamo with an extended inertial range of turbulence and in diverse plasma conditions. This can result in discrepancies between theoretical predictions and simulations on the dynamo behavior and magnetic field structure. For instance, the peak scale of magnetic energy spectrum, which was believed to be close to the resistive scale based on earlier low-resolution dynamo simulations with insufficient turbulent inertial range (e.g., [84]), has been shown to be significantly distant from the resistive scale by higher-resolution dynamo simulations (e.g., [14]).

Conflict of interest

The authors declare that they have no conflict of interest.

References

1. C.F. McKee, E.C. Ostriker, *Ann. Rep. A&A* **45**, 565 (2007). DOI 10.1146/annurev.astro.45.051806.110602
2. A. Brandenburg, A. Lazarian, *SSR*(2013). DOI 10.1007/s11214-013-0009-3
3. A. Lazarian, G.L. Eyink, A. Jafari, G. Kowal, H. Li, S. Xu, E.T. Vishniac, *Physics of Plasmas* **27**(1), 012305 (2020). DOI 10.1063/1.5110603
4. A. Brandenburg, K. Subramanian, *Phys. Rep.* **417**, 1 (2005). DOI 10.1016/j.physrep.2005.06.005
5. R.J. Leamon, C.W. Smith, N.F. Ness, W.H. Matthaeus, H.K. Wong, *JGR***103**, 4775 (1998). DOI 10.1029/97JA03394
6. D. Ryu, H. Kang, J. Cho, S. Das, *Science* **320**, 909 (2008). DOI 10.1126/science.1154923
7. F. Miniati, A. Beresnyak, *Nature***523**(7558), 59 (2015). DOI 10.1038/nature14552
8. F. Marinacci, M. Vogelsberger, R. Pakmor, P. Torrey, V. Springel, L. Hernquist, D. Nelson, R. Weinberger, A. Pillepich, J. Naiman, S. Genel, *MNRAS* **480**(4), 5113 (2018). DOI 10.1093/mnras/sty2206
9. P. Domínguez-Fernández, F. Vazza, M. Brügggen, G. Brunetti, *MNRAS* **486**(1), 623 (2019). DOI 10.1093/mnras/stz877
10. S. Sur, C. Federrath, D.R.G. Schleicher, R. Banerjee, R.S. Klessen, *MNRAS* **423**, 3148 (2012). DOI 10.1111/j.1365-2966.2012.21100.x
11. J. Schober, D.R.G. Schleicher, R.S. Klessen, *A&A* **560**, A87 (2013). DOI 10.1051/0004-6361/201322185
12. C.F. McKee, A. Stacy, P.S. Li, *MNRAS* **496**(4), 5528 (2020). DOI 10.1093/mnras/staa1903
13. S. Xu, A. Lazarian, *Astrophys. J.***899**(2), 115 (2020). DOI 10.3847/1538-4357/aba7ba
14. N.E. Haugen, A. Brandenburg, W. Dobler, *Phys. Rev. E***70**(1), 016308 (2004). DOI 10.1103/PhysRevE.70.016308
15. G.K. Batchelor, *Royal Society of London Proceedings Series A* **201**, 405 (1950). DOI 10.1098/rspa.1950.0069
16. A.P. Kazantsev, *Soviet Journal of Experimental and Theoretical Physics* **26**, 1031 (1968)
17. R.M. Kulsrud, S.W. Anderson, *Astrophys. J.***396**, 606 (1992). DOI 10.1086/171743
18. K. Subramanian, *MNRAS* **294**, 718 (1998). DOI 10.1046/j.1365-8711.1998.01284.x
19. A.A. Schekochihin, S.C. Cowley, S.F. Taylor, J.L. Maron, J.C. McWilliams, *Astrophys. J.***612**, 276 (2004). DOI 10.1086/422547
20. K. Subramanian, *ArXiv Astrophysics* 9708216 (1997)
21. A. Brandenburg, M. Rempel, *Astrophys. J.***879**(1), 57 (2019). DOI 10.3847/1538-4357/ab24bd
22. A. Brandenburg, *MNRAS* **487**(2), 2673 (2019). DOI 10.1093/mnras/stz1509
23. J. Cho, E.T. Vishniac, *Astrophys. J.***538**(1), 217 (2000). DOI 10.1086/309127
24. N.E.L. Haugen, A. Brandenburg, W. Dobler, *ApJ* **597**(2), L141 (2003). DOI 10.1086/380189

25. J. Cho, E.T. Vishniac, A. Beresnyak, A. Lazarian, D. Ryu, *Astrophys. J.* **693**, 1449 (2009). DOI 10.1088/0004-637X/693/2/1449
26. A. Beresnyak, *Physical Review Letters* **108**(3), 035002 (2012). DOI 10.1103/PhysRevLett.108.035002
27. S. Xu, A. Lazarian, *Astrophys. J.* **833**, 215 (2016). DOI 10.3847/1538-4357/833/2/215
28. A. Lazarian, E.T. Vishniac, *Astrophys. J.* **517**, 700 (1999). DOI 10.1086/307233
29. A. Lazarian, in *Magnetic Fields in the Universe: From Laboratory and Stars to Primordial Structures.*, *American Institute of Physics Conference Series*, vol. 784, ed. by E.M. de Gouveia dal Pino, G. Lugones, A. Lazarian (2005), *American Institute of Physics Conference Series*, vol. 784, pp. 42–53. DOI 10.1063/1.2077170
30. G.L. Eyink, A. Lazarian, E.T. Vishniac, *Astrophys. J.* **743**, 51 (2011). DOI 10.1088/0004-637X/743/1/51
31. G.L. Eyink, *Astrophys. J.* **807**(2), 137 (2015). DOI 10.1088/0004-637X/807/2/137
32. S. Xu, S.K. Garain, D.S. Balsara, A. Lazarian, *Astrophys. J.* **872**(1), 62 (2019). DOI 10.3847/1538-4357/aafbe8
33. L. Biermann, *Zeitschrift Naturforschung Teil A* **5**, 65 (1950)
34. J.M. Quashnock, A. Loeb, D.N. Spergel, *ApJ* **344**, L49 (1989). DOI 10.1086/185528
35. A. Lazarian, *A&A* **264**(1), 326 (1992)
36. G. Sigl, A.V. Olinto, K. Jedamzik, *Phys. Rev. D* **55**, 4582 (1997). DOI 10.1103/PhysRevD.55.4582
37. R. Schlickeiser, U. Kolberg, P.H. Yoon, *Astrophys. J.* **857**(1), 29 (2018). DOI 10.3847/1538-4357/aab3dd
38. S. Xu, A. Lazarian, *Astrophys. J.* **850**(2), 126 (2017). DOI 10.3847/1538-4357/aa956b
39. S. Xu, A. Lazarian, *New Journal of Physics* **19**(6), 065005 (2017). DOI 10.1088/1367-2630/aa6ec9
40. R.H. Kraichnan, S. Nagarajan, *Physics of Fluids* **10**, 859 (1967). DOI 10.1063/1.1762201
41. G.L. Eyink, *Phys. Rev. E* **82**(4), 046314 (2010). DOI 10.1103/PhysRevE.82.046314
42. R. Santos-Lima, A. Lazarian, E.M. de Gouveia Dal Pino, J. Cho, *Astrophys. J.* **714**, 442 (2010). DOI 10.1088/0004-637X/714/1/442
43. A. Lazarian, A. Esquivel, R. Crutcher, *Astrophys. J.* **757**, 154 (2012). DOI 10.1088/0004-637X/757/2/154
44. A. Lazarian, *SSR* **181**, 1 (2014). DOI 10.1007/s11214-013-0031-5
45. A.V. Chepurinov, *Astronomical and Astrophysical Transactions* **17**(4), 281 (1998). DOI 10.1080/10556799808232095
46. C. Vogt, T.A. Enßlin, *A&A* **434**(1), 67 (2005). DOI 10.1051/0004-6361:20041839
47. P. Padoan, L. Pan, T. Haugbølle, Å. Nordlund, *Astrophys. J.* **822**, 11 (2016). DOI 10.3847/0004-637X/822/1/11
48. S. Xu, A. Lazarian, H. Yan, *Astrophys. J.* **810**, 44 (2015). DOI 10.1088/0004-637X/810/1/44
49. S. Xu, H. Yan, A. Lazarian, *Astrophys. J.* **826**, 166 (2016). DOI 10.3847/0004-637X/826/2/166
50. B.G. Elmegreen, *Astrophys. J.* **530**, 277 (2000). DOI 10.1086/308361
51. R.M. Crutcher, *Ann. Rep. A&A* **50**, 29 (2012). DOI 10.1146/annurev-astro-081811-125514
52. M.S. Longair, *High energy astrophysics. Volume 2. Stars, the Galaxy and the interstellar medium.* (1994)
53. A. Bamba, R. Yamazaki, J.S. Hiraga, *Astrophys. J.* **632**, 294 (2005). DOI 10.1086/432711
54. J. Vink, *AAPR* **20**, 49 (2012). DOI 10.1007/s00159-011-0049-1
55. T. Inoue, R. Yamazaki, S.i. Inutsuka, *Astrophys. J.* **695**, 825 (2009). DOI 10.1088/0004-637X/695/2/825
56. Y. Uchiyama, F.A. Aharonian, T. Tanaka, T. Takahashi, Y. Maeda, *Nature* **449**, 576 (2007). DOI 10.1038/nature06210
57. Y. Uchiyama, F.A. Aharonian, *ApJ* **677**, L105 (2008). DOI 10.1086/588190
58. L. Spitzer, *Diffuse matter in space* (1968)
59. P. Girichidis, L. Konstandin, A.P. Whitworth, R.S. Klessen, *Astrophys. J.* **781**(2), 91 (2014). DOI 10.1088/0004-637X/781/2/91
60. P. Sharda, C. Federrath, M.R. Krumholz, arXiv:2002.11502 arXiv:2002.11502 (2020)
61. B. Robertson, P. Goldreich, *ApJ* **750**, L31 (2012). DOI 10.1088/2041-8205/750/2/L31
62. E.J. Lee, P. Chang, N. Murray, *Astrophys. J.* **800**, 49 (2015). DOI 10.1088/0004-637X/800/1/49
63. S. Xu, A. Lazarian, *Astrophys. J.* **890**(2), 157 (2020). DOI 10.3847/1538-4357/ab6e63
64. B.T. Draine, *MNRAS* **220**, 133 (1986). DOI 10.1093/mnras/220.1.133
65. D.S. Balsara, *ApJ* **116**, 119 (1998). DOI 10.1086/313092
66. D.S. Balsara, *ApJ* **116**, 133 (1998). DOI 10.1086/313093

67. F.H. Shu, *The physics of astrophysics. Volume II: Gas dynamics.* (1992)
68. R. Blandford, D. Eichler, *Phys. Rep.* **154**, 1 (1987). DOI 10.1016/0370-1573(87)90134-7
69. A.R. Bell, *MNRAS* **353**, 550 (2004). DOI 10.1111/j.1365-2966.2004.08097.x
70. A. Beresnyak, T.W. Jones, A. Lazarian, *Astrophys. J.* **707**, 1541 (2009). DOI 10.1088/0004-637X/707/2/1541
71. L.O. Drury, T.P. Downes, *MNRAS* **427**, 2308 (2012). DOI 10.1111/j.1365-2966.2012.22106.x
72. M.V. del Valle, A. Lazarian, R. Santos-Lima, *MNRAS* **458**, 1645 (2016). DOI 10.1093/mnras/stw340
73. S. Xu, B. Zhang, *Astrophys. J.* **835**, 2 (2017). DOI 10.3847/1538-4357/835/1/2
74. S. Xu, B. Zhang, arXiv:2011.01244 arXiv:2011.01244 (2020)
75. C. Heiles, T.H. Troland, *Astrophys. J.* **586**, 1067 (2003). DOI 10.1086/367828
76. A.A. Goodman, J.A. Barranco, D.J. Wilner, M.H. Heyer, *Astrophys. J.* **504**, 223 (1998). DOI 10.1086/306045
77. B.T. Draine, A. Lazarian, *ApJ* **494**, L19 (1998). DOI 10.1086/311167
78. A. Bamba, R. Yamazaki, M. Ueno, K. Koyama, *Astrophys. J.* **589**, 827 (2003). DOI 10.1086/374687
79. A. Bamba, R. Yamazaki, T. Yoshida, T. Terasawa, K. Koyama, *Astrophys. J.* **621**, 793 (2005). DOI 10.1086/427620
80. M.L. Ahnen, S. Ansoldi, L.A. Antonelli, C. Arcaro, A. Babić, B. Banerjee, P. Bangale, U. Barres de Almeida, J.A. Barrio, J. Becerra González, W. Bednarek, E. Bernardini, A. Berti, W. Bhattacharyya, B. Biasuzzi, A. Biland, O. Blanch, S. Bonnefoy, G. Bonnoli, R. Carosi, A. Carosi, A. Chatterjee, M. Colak, P. Colin, E. Colombo, J.L. Contreras, J. Cortina, S. Covino, P. Cumani, P. Da Vela, F. Dazzi, A. De Angelis, B. De Lotto, E. de Oña Wilhelmi, F. Di Pierro, M. Doert, A. Domínguez, D. Dominis Prester, D. Dorner, M. Doro, S. Einecke, D. Eisenacher Glawion, D. Elsaesser, M. Engelkemeier, V. Fallah Ramazani, A. Fernández-Barral, D. Fidalgo, M.V. Fonseca, L. Font, C. Fruck, D. Galindo, R.J. García López, M. Garczarczyk, M. Gaug, P. Giammaria, N. Godinović, D. Gora, D. Guberman, D. Hadasch, A. Hahn, T. Hassan, M. Hayashida, J. Herrera, J. Hose, D. Hrupec, T. Inada, K. Ishio, Y. Konno, H. Kubo, J. Kushida, D. Kuveždić, D. Lelas, E. Lindfors, S. Lombardi, F. Longo, M. López, C. Maggio, P. Majumdar, M. Makariev, G. Maneva, M. Manganaro, K. Mannheim, L. Maraschi, M. Mariotti, M. Martínez, D. Mazin, U. Menzel, M. Minev, R. Mirzoyan, A. Moralejo, V. Moreno, E. Moretti, V. Neustroev, A. Niedzwiecki, M. Nieves Rosillo, K. Nilsson, D. Ninci, K. Nishijima, K. Noda, L. Nogués, S. Paiano, J. Palacio, D. Paneque, R. Paoletti, J.M. Paredes, G. Pedalletti, M. Peresano, L. Perri, M. Persic, P.G. Prada Moroni, E. Prandini, I. Puljak, J.R. Garcia, I. Reichardt, W. Rhode, M. Ribó, J. Rico, C. Righi, T. Saito, K. Satalecka, S. Schroeder, T. Schweizer, S.N. Shore, J. Sitarek, I. Šnidarić, D. Sobczynska, A. Stamera, M. Strzys, T. Surić, L. Takalo, F. Tavecchio, P. Temnikov, T. Terzić, D. Tescaro, M. Teshima, N. Torres-Albà, A. Treves, G. Vanzo, M. Vazquez Acosta, I. Vovk, J.E. Ward, M. Will, D. Zarić, *MNRAS* **472**(3), 2956 (2017). DOI 10.1093/mnras/stx2079
81. H. E. S. S. Collaboration, H. Abdalla, A. Abramowski, F. Aharonian, F. Ait Benkhali, A.G. Akhperjanian, T. Andersson, E.O. Angüner, M. Arrieta, P. Aubert, M. Backes, A. Balzer, M. Barnard, Y. Becherini, J. Becker Tjus, D. Berge, S. Bernhard, K. Bernlöhr, R. Blackwell, M. Böttcher, C. Boisson, J. Bolmont, P. Bordas, J. Bregeon, F. Brun, P. Brun, M. Bryan, T. Bulik, M. Capasso, J. Carr, S. Casanova, M. Cerruti, N. Chakraborty, R. Chalme-Calvet, R.C.G. Chaves, A. Chen, J. Chevalier, M. Chrétiens, S. Colafrancesco, G. Cologna, B. Condon, J. Conrad, Y. Cui, I.D. Davids, J. De Cock, B. Degrange, C. Deil, J. Devin, P. deWilt, L. Dirson, A. Djannati-Ataï, W. Domainko, A. Donath, L.O.C. Drury, G. Dubus, K. Dutton, J. Dyks, T. Edwards, K. Egberts, P. Eger, J.P. Ermenwein, S. Eschbach, C. Farnier, S. Fegan, M.V. Fernandes, A. Fiasson, G. Fontaine, A. Förster, T. Fukuyama, S. Funk, M. Füßling, S. Gabici, M. Gajdus, Y.A. Gallant, T. Garrigoux, G. Giavitto, B. Giebels, J.F. Glicenstein, D. Gottschall, A. Goyal, M.H. Grondin, D. Hadasch, J. Hahn, M. Haupt, J. Hawkes, G. Heinzlmann, G. Henri, G. Hermann, O. Hervet, J.A. Hinton, W. Hofmann, C. Hoischen, M. Holler, D. Horns, A. Ivascenko, A. Jacholkowska, M. Jamroz, M. Janiak, D. Jankowsky, F. Jankowsky, M. Jingo, T. Jogler, L. Jouvin, I. Jung-Richardt, M.A. Kastendieck, K. Katarzyński, U. Katz, D. Kerszberg, B. Khélifi, M. Kieffer, J. King, S. Klepser, D. Klochkov, W. Kluźniak, D. Kolitzus, N. Komin, K. Kosack, S. Krakau, M. Kraus, F. Krayzel, P.P. Krüger, H. Laffon, G. Lamanna, J. Lau, J.P. Lees, J. Lefaucheur, V. Lefranc, A. Lemièvre, M. Lemoine-Goumard, J.P. Lenain, E. Leser, T. Lohse, M. Lorentz, R. Liu, R. López-Coto, I. Lypova, V. Marandon, A. Marcowith, C. Mariaud, R. Marx, G. Maurin, N. Maxted, M. Mayer, P.J. Meintjes, M. Meyer, A.M.W. Mitchell, R. Moderski, M. Mohamed, L. Mohrmann, K. Morå, E. Moulin, T. Murach, M. de Naurois, F. Niederwanger, J. Niemiec, L. Oakes, P. O'Brien, H. Odaka, S. Öttl, S. Ohm, M. Ostrowski, I. Oya, M. Padovani, M. Panter, R.D. Parsons, N.W. Pekeur, G. Pelletier, C. Perennes, P.O.

- Petrucci, B. Peyaud, Q. Piel, S. Pita, H. Poon, D. Prokhorov, H. Prokoph, G. Pühlhofer, M. Punch, A. Quirrenbach, S. Raab, A. Reimer, O. Reimer, M. Renaud, R. de los Reyes, F. Rieger, C. Romoli, S. Rosier-Lees, G. Rowell, B. Rudak, C.B. Rulten, V. Sahakian, D. Salek, D.A. Sanchez, A. Santangelo, M. Sasaki, R. Schlickeiser, F. Schüssler, A. Schulz, U. Schwanke, S. Schwemmer, M. Settimo, A.S. Seyffert, N. Shafi, I. Shilon, R. Simoni, H. Sol, F. Spanier, G. Spengler, F. Spies, Ł. Stawarz, R. Steenkamp, C. Stegmann, F. Stinzing, K. Stycz, I. Sushch, T. Takahashi, J.P. Tavernet, T. Tavernier, A.M. Taylor, R. Terrier, L. Tibaldo, D. Tiziani, M. Tluczykont, C. Trichard, R. Tuffs, Y. Uchiyama, D.J. van der Walt, C. van Eldik, C. van Rensburg, B. van Soelen, G. Vasileiadis, J. Veh, C. Venter, A. Viana, P. Vincent, J. Vink, F. Voisin, H.J. Völk, F. Volpe, T. Vuillaume, Z. Wadiasingh, S.J. Wagner, P. Wagner, R.M. Wagner, R. White, A. Wierzholska, P. Willmann, A. Wörnlein, D. Wouters, R. Yang, V. Zabalza, D. Zaborov, M. Zacharias, A.A. Zdziarski, A. Zech, F. Zefi, A. Ziegler, N. Żywucka, *A&A* **612**, A6 (2018). DOI 10.1051/0004-6361/201629790
82. J. Schober, D. Schleicher, C. Federrath, S. Glover, R.S. Klessen, R. Banerjee, *Astrophys. J.* **754**, 99 (2012). DOI 10.1088/0004-637X/754/2/99
83. P. Goldreich, S. Sridhar, *Astrophys. J.* **438**, 763 (1995). DOI 10.1086/175121
84. J. Maron, S. Cowley, J. McWilliams, *Astrophys. J.* **603**(2), 569 (2004). DOI 10.1086/380504

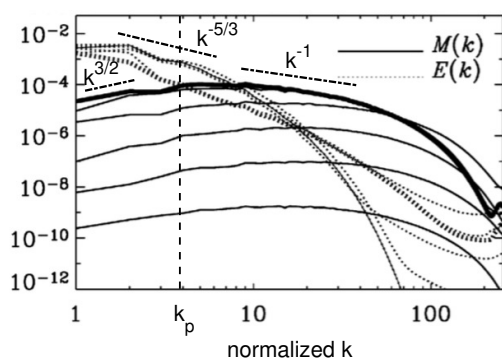
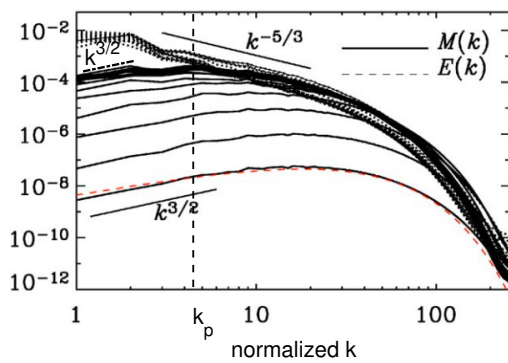
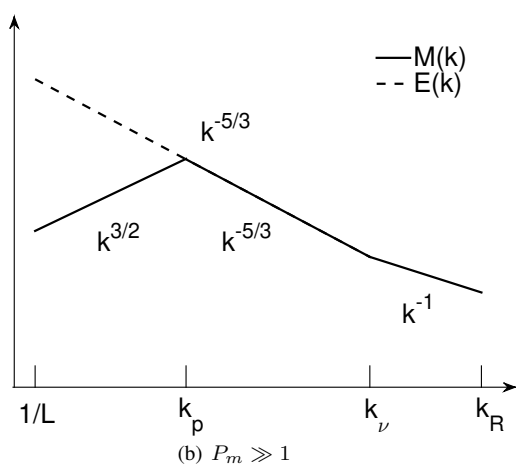
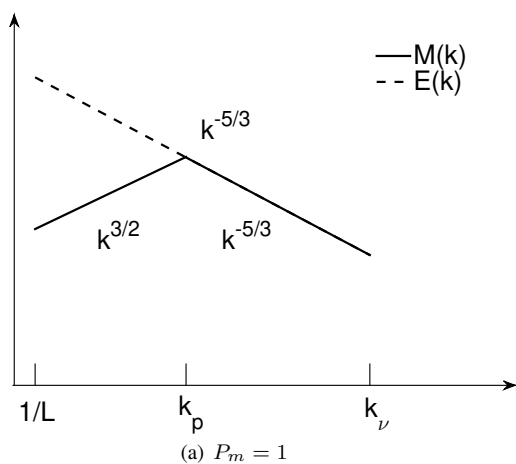


Fig. 1 Comparison between the analytical expectation (a,b) and numerical simulation (c,d) on the magnetic energy spectrum $M(k)$ during the nonlinear stage of dynamo at $P_m = 1$ and $P_m \gg 1$. $E(k)$ is turbulent energy spectrum. From XL16.

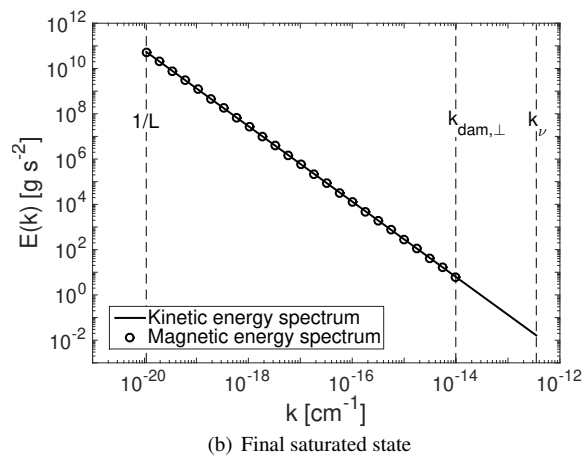
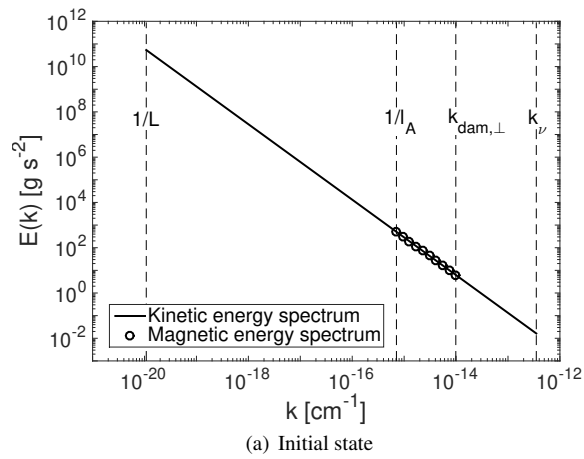


Fig. 2 Magnetic energy spectrum at the initial state (a) and final state (b) of the nonlinear turbulent dynamo in an initially super-Alfvénic MC. From [39].

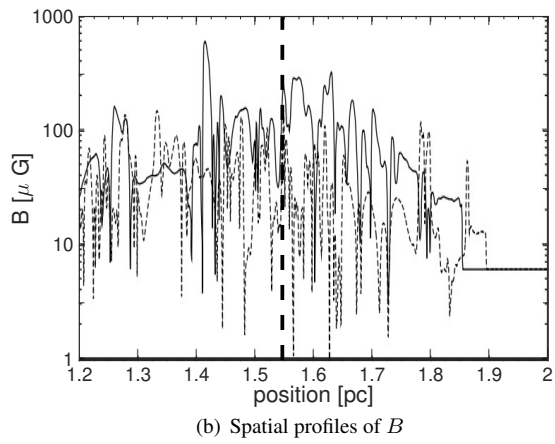
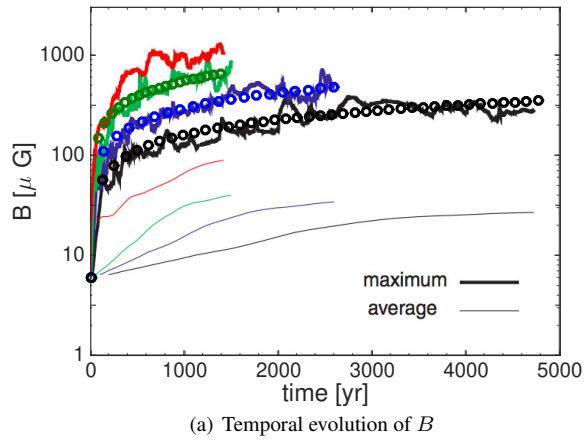


Fig. 3 Comparisons between the nonlinear dynamo theory (XL16) and the numerical results in [55] for magnetic field amplification in the SNR postshock region. The circles in (a) and the vertical dashed line in (b) are analytical calculations. From [38].

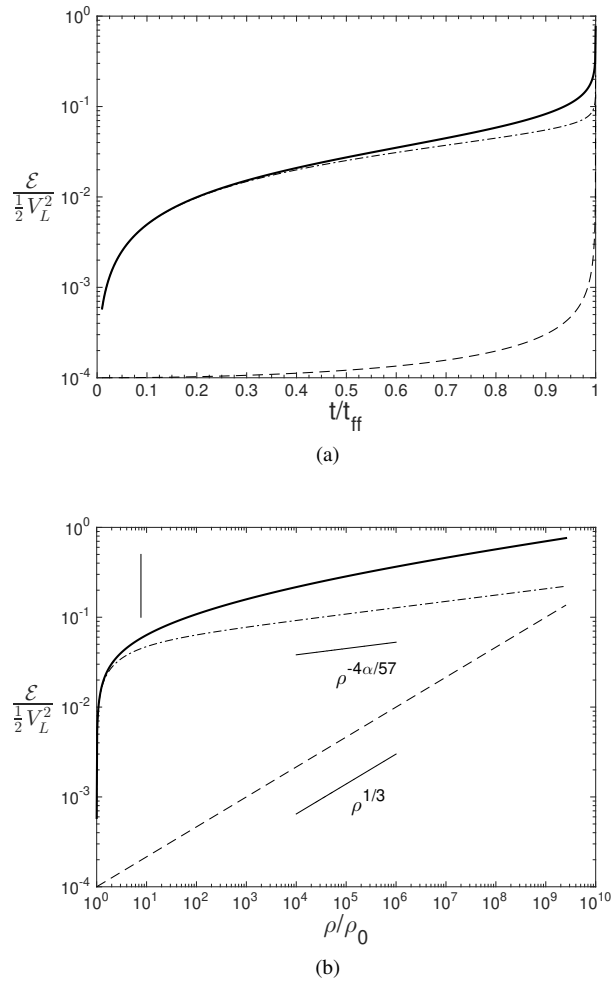


Fig. 4 Normalized \mathcal{E} as a function of normalized t in (a) and as a function of normalized ρ in (b). The solid line is given by Eq. (8) when the reconnection diffusion of magnetic fields is considered. The dash-dotted line is its approximation given by Eq. (9). The dashed line shows the flux-freezing scaling as a comparison (Eq. (12)). The short vertical line in (b) corresponds to $t/t_{ff} = 0.8$. From [13].

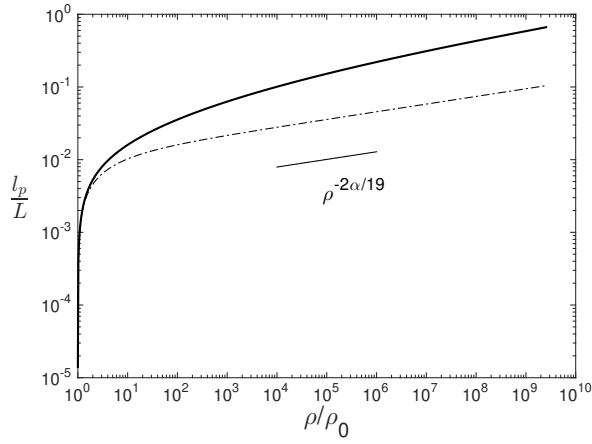


Fig. 5 Normalized l_p as a function of normalized ρ . The solid line is given by Eq. (15). The dash-dotted line is its approximation corresponding to the approximate expression of \mathcal{E} (the dash-dotted line in Fig. 4). From [13].

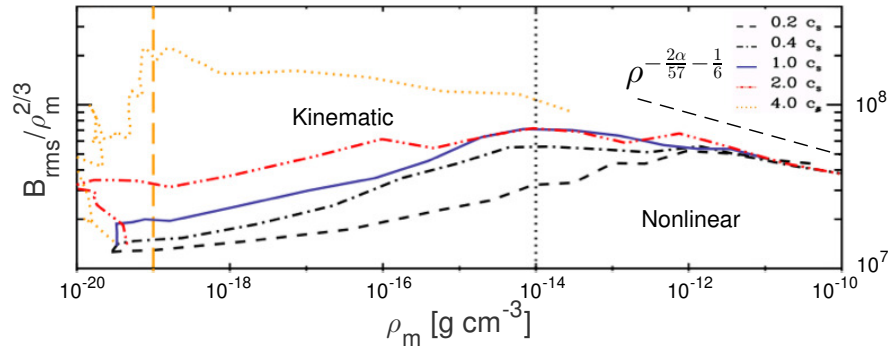


Fig. 6 Comparison between the theory by [13] and the numerical result in [10] on the evolution of magnetic field strength as a function of density during gravitational collapse. For the numerical result in [10], different colors represent the numerical runs with different initial turbulent velocities, $v_{tur,0} = 0.2, 0.4, 1.0, 2.0, 4.0 c_s$, where c_s is the sound speed. The yellow dashed vertical line for $v_{tur,0} = 4.0 c_s$ and the black dotted vertical line for other values of $v_{tur,0}$ indicate the transition from the kinematic to nonlinear dynamo regime. From [13].

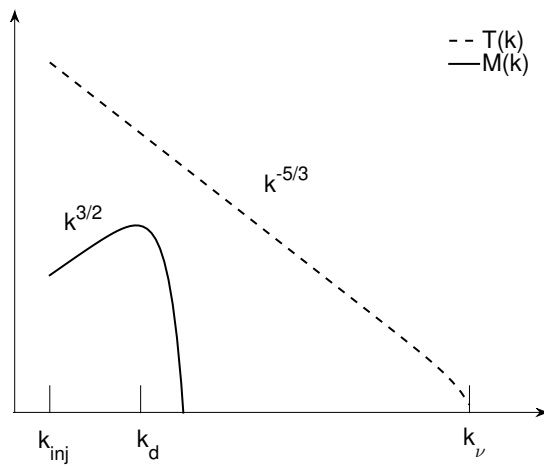


Fig. 7 Illustration for the magnetic energy spectrum $M(k)$ and the turbulent energy spectrum $T(k)$ in the damping stage of turbulent dynamo. From [32].

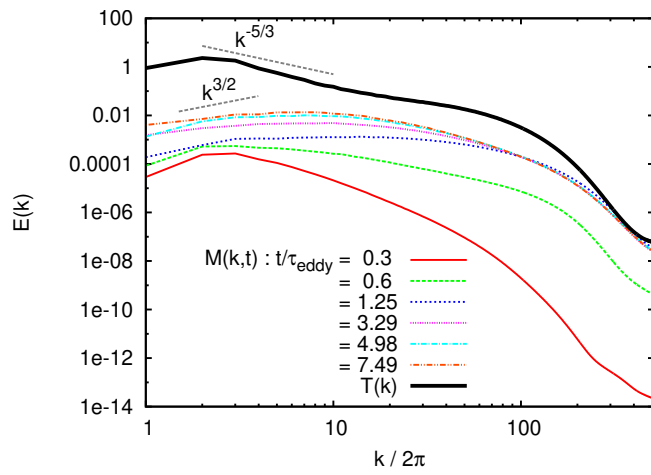


Fig. 8 Numerically measured $M(k, t)$ at different times during the two-fluid dynamo simulation. $T(k)$ is the energy spectrum of driven turbulence. From [32].

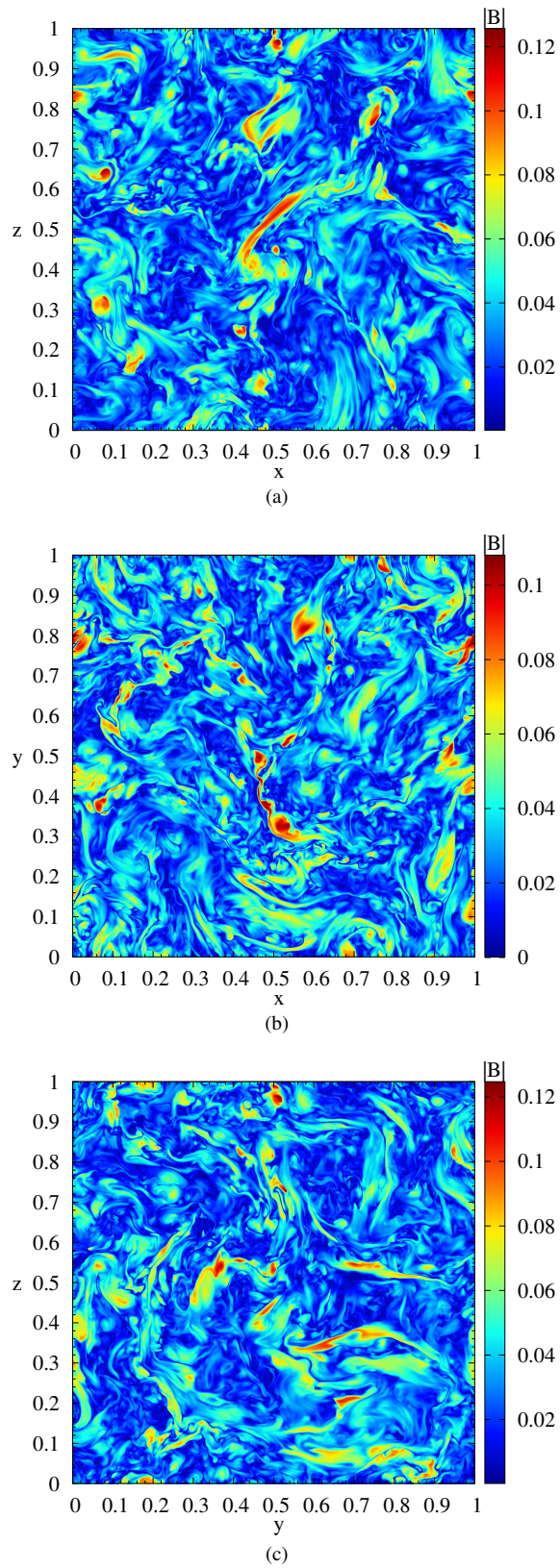


Fig. 9 2D cross sections of the numerically measured magnetic field strength in the (a) xz plane, (b) xy plane, and (c) yz plane at $t = 7.49 \tau_{\text{eddy}}$. From [32].

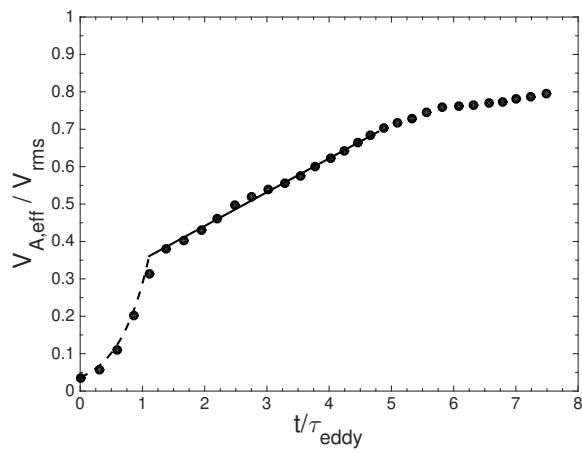


Fig. 10 Time evolution of the numerically measured $V_{A,\text{eff}}$ (normalized by V_{rms} , circles) in comparison with the theoretical prediction (solid line). From [32].

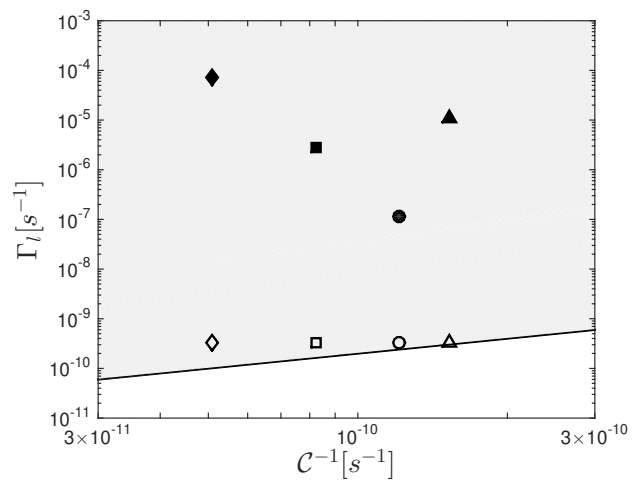


Fig. 11 Dynamo stretching rate Γ vs. C^{-1} for the turbulent dynamo in the shock precursor in the WNM (circle), CNM (square), MC (triangle), and DC (diamond). The shaded region shows the parameter space for the damping stage of dynamo. Filled and open symbols represent Γ at the viscous scale and L , respectively. From [32].

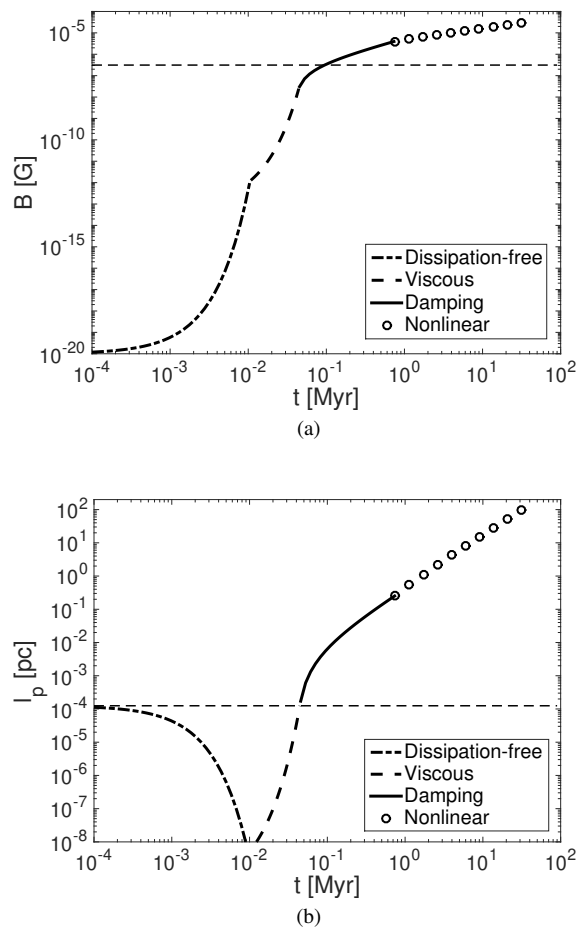


Fig. 12 Time evolution of the magnetic field strength and the correlation length of the amplified magnetic fields during the formation of the first galaxies. From XL16.